CPDM: Content-Preserving Diffusion Model for Underwater Image Enhancement

Xiaowen Shi and Yuan-Gen Wang

School of Computer Science and Cyber Engineering, Guangzhou University, China
shixiaowen@e.gzhu.edu.cn, wangyg@gzhu.edu.cn

arXiv:2401.15649v1 [cs.CV] 28 Jan 2024

Abstract

Underwater image enhancement (UIE) is challenging since image degradation in aquatic environments is complicated and changing over time. Existing mainstream methods rely on either physical-model or data-driven, suffering from performance bottlenecks due to changes in imaging conditions or training instability. In this article, we make the first attempt to adapt the diffusion model to the UIE task and propose a Content-Preserving Diffusion Model (CPDM) to address the above challenges. CPDM first leverages a diffusion model as its fundamental model for stable training and then designs a content-preserving framework to deal with changes in imaging conditions. Specifically, we construct a conditional input module by adopting both the raw image and the difference between the raw and noisy images as the input, which can enhance the model's adaptability by considering the changes involving the raw images in underwater environments. To preserve the essential content of the raw images, we construct a content compensation module for content-aware training by extracting low-level features from the raw images. Extensive experimental results validate the effectiveness of our CPDM, surpassing the state-of-the-art methods in terms of both subjective and objective metrics.

Introduction

Underwater image enhancement (UIE) has gained great attention recently as human activities have increasingly ventured into the ocean. However, enhancing the quality of degraded underwater images poses significant challenges due to the complex and ever-changing underwater environment, as well as poor lighting conditions. The degradation of underwater images is primarily caused by the selective absorption and scattering of visible light wavelengths within the underwater environment (McGlamery 1980; Jaffe 1990; Hou et al. 2012; Akkaynak et al. 2017; Akkaynak and Treibitz 2018). Consequently, the acquired underwater images exhibit low contrast, low brightness, significant color deviations, blurred details, uneven bright spots, and other defects. These limitations greatly hinder practical applications in fields such as marine ecology (Strachan 1993), marine biology and archaeology (Ludvigsen et al. 2007), remotely operated vehicles,

and autonomous underwater vehicles (Johnsen et al. 2016; Ahn et al. 2017). Therefore, the study of UIE holds immense significance for advancing related underwater research.

Some UIE techniques have been developed for enhancing the quality of underwater images, which can be roughly categorized into physical-model and data-driven methods. Physical-model methods (Galdran et al. 2015; Li et al. 2016; Drews et al. 2016; Li et al. 2017a; Peng and Cosman 2017; Wang, Liu, and Chau 2017; Peng, Cao, and Cosman 2018; Akkaynak and Treibitz 2019) aim to model the physical process of light propagation in water by taking absorption, scattering, and other optical properties of the underwater environment into account. These methods often involve complex mathematical models and algorithms to simulate degradation. However, since the aquatic environments change over time, the method established in a certain physical scenario cannot adapt to other different physical scenarios, resulting in poor generalization.

Motivated by the success of deep learning in a wide range of fields, data-driven methods (Li et al. 2017b; Li, Guo, and Guo 2018; Guo, Li, and Zhuang 2019; Li et al. 2021; Fu et al. 2022; Peng, Zhu, and Bian 2023) have been proposed by learning the mapping between degraded underwater images and their corresponding high-quality reference images. These methods rely on large-scale datasets for model training, effectively enhancing image quality based on learned patterns and features. However, currently established UIE datasets are generally collected in a specific underwater environment, such as low lighting, various turbidity, and different densities of particulate matter. Hence, the model trained on a single dataset suffers from poor cross-dataset performance.

In this work, we propose a novel UIE framework, termed Content-Preserving Diffusion Model (CPDM), for enhancing the quality of underwater images. Specifically, we utilize the raw image as a conditional input during the model training process. To facilitate the extraction of differential features at different time steps, we introduce the differences between the raw image and the noisy image at each time step as another conditional input. Furthermore, to ensure that the model preserves the essential content of raw images, we design a content compensation module to extract the low-level features of raw images for content-aware training. Figure 1 provides a preview of the enhancement results achieved by our CPDM. The main contributions of this article are as follows:
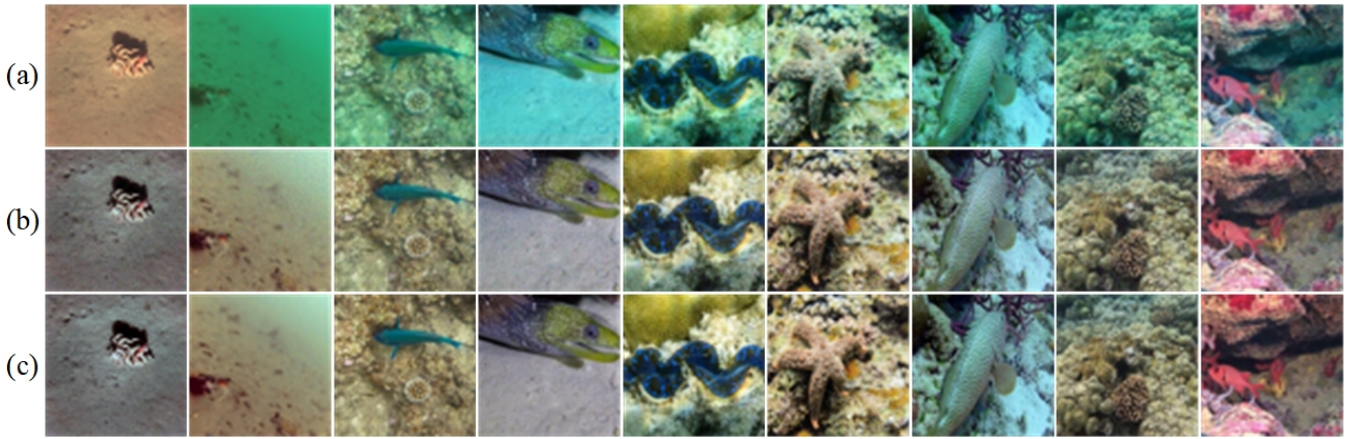
Figure 1: A visual illustration of the proposed CPDM method. (a) Original images to be enhanced. (b) Images enhanced by our CPDM. (c) Reference images as ground truth.

- We present a Content-Preserving Diffusion Model (CPDM) for underwater image enhancement (UIE). To adapt the diffusion model to such a new task, we take the raw image as conditional input for training at each time step, enabling the restored target image to have consistent content with the raw image.

- We introduce the difference between the raw image and the noisy image of the current time step as an extra conditional input for content-aware training at the current time step, iteratively refining the output of each time step and resulting in a high-quality enhanced target image.

- We design a content compensation module to ensure that the trained model preserves the low-level features of raw images, such as structure, texture, and edge, preventing excessive modification of these important details within the images.

- Extensive experimental results show that our CPDM outperforms state-of-the-art methods. The ablation study also demonstrates the effectiveness of each module designed in this work. Especially, the proposed CPDM achieves good generalization and greatly improves color fidelity.

Related Work

Underwater Image Enhancement Methods

Methods for underwater image enhancement play a crucial role in improving the visual quality of underwater images. The existing mainstream methods mainly consist of physical-model and data-driven (Li et al. 2019).

Physical-model. Physical-model methods treat underwater image enhancement as an inverse problem. These methods involve several steps: constructing a physical model to simulate the degradation process, estimating unknown model parameters based on the given images, and solving the inverse problem using the estimated parameters. By solving the inverse problem, these methods can enhance underwater image quality, mitigating the impact of degradation factors such as light attenuation, scattering, and color distortion. Drews et al. (Drews et al. 2016) introduced the Underwater Dark

Channel Prior method, addressing the issue of the unreliable red channel in underwater images. Liu et al. (Liu and Chau 2016) formulated a cost function based on the observation that the dark channel of underwater images tends to zero and minimized it to find the optimal transmission mapping that maximizes image contrast. Peng et al. (Peng and Cosman 2017) proposed a method for enhancing underwater images by estimating image blur and depth. Peng et al. (Peng, Cao, and Cosman 2018) introduced the Generalized Dark Channel Prior to image restoration, which incorporates adaptive color correction into the image formation model. Akkaynak et al. (Akkaynak and Treibitz 2019) presented a modified underwater color correction method for enhancing underwater images.

Data-driven. In comparison to physical-model methods, data-driven methods for underwater image enhancement have been developed lately (Paulo Drews et al. 2013; Yang et al. 2019). Since the effectiveness of underwater image enhancement is influenced by specific factors such as scene, lighting condition, temperature, and turbidity, it is challenging to employ synthetic and realistic underwater images for network training. Moreover, neural networks trained on synthetic underwater images may not generalize well to real-world scenarios. WaterGAN (Li et al. 2017b) utilized in-air images and depth maps as input to generate synthetic underwater images as output. These synthetic underwater images are then used for color correction of monocular underwater images. Water CycleGAN (Li, Guo, and Guo 2018) relaxed the requirement of paired underwater images by utilizing a weakly-supervised color transfer approach to correct color distortions. However, it may generate unrealistic results. Guo et al. (Guo, Li, and Zhuang 2019) proposed a multi-scale dense GAN for underwater image enhancement. However, this method still cannot overcome the limitations of unpredicted outputs from GANs (Goodfellow et al. 2014). Ucolor (Li et al. 2021) integrated an underwater physical imaging model and a medium transmission-guided model to enhance image quality in regions with severe degradation. However, the performance of the approach is significantly affected by different underwater environments. U-shape (Peng, Zhu, and

Bian 2023) proposed a U-shape Transformer with integrated modules to reinforce the network's attention to color channels and spatial areas that suffer from severe attenuation. This model includes a channel-wise multi-scale feature fusion transformer module and a spatial-wise global feature modeling transformer module. However, this method still exhibits major color distortion.

Diffusion Model for Image Generation

As a generative model, the diffusion model has demonstrated impressive performance in numerous computer vision tasks. According to the presence or absence of conditions, the diffusion model can be categorized into conditional diffusion and unconditional diffusion (Croitoru et al. 2023).

Unconditional Diffusion. Denoising Diffusion Probabilistic Model (DDPM) (Ho, Jain, and Abbeel 2020; Sohl-Dickstein et al. 2015) draw inspiration from non-equilibrium thermodynamics (Jarzynski and C. 1997) and are composed of two processes: forward noising process and backward denoising process. In the forward process, DDPM applies a Markov chain-based diffusion to gradually introduce noise into the original image until its distribution aligns with a standard Gaussian distribution. The backward process is the inverse of the forward process, where a sample is drawn from a standard Gaussian distribution, and the noise introduced during the forward process is gradually eliminated, resulting in the gradual generation of the target image. Denoising Diffusion Implicit Model (DDIM) (Song, Meng, and Ermon 2020) optimizes the sampling process in DDPM by transforming it into a non-Markovian process and enhancing sampling efficiency. The training process remains unchanged, while significant optimizations are made to the steps in the sampling process.

Conditional Diffusion. Conditional diffusion models are built upon the diffusion model and incorporate additional conditions, such as category, text, and image, to guide the diffusion and generation processes. Guided diffusion (Dhariwal and Nichol 2021) utilizes a classifier to classify the generated images, calculates gradients based on the cross-entropy loss between the classification score and the target category, and then employs these gradients to guide the next sampling. A notable advantage of this method is that it does not require retraining the diffusion model. Instead, guidance is added during the forward process to achieve the desired generation effect. Semantic guidance diffusion (SGD) (Liu et al. 2023) introduces two forms of category guidance: reference graph-based guidance and text-based guidance. By designing corresponding gradient terms, the SGD method achieves specific guidance effects tailored to these different forms of category guidance. (Li et al. 2023) applied the conditional diffusion model to unsupervised despeckling for AS-OCT images.

Proposed method

This section provides a detailed description of the proposed Content-Preserving Diffusion Model (CPDM). Our CPDM includes the conditional input and content compensation modules, which are shown in Figures 2 and 3. In the following, we will describe these two modules in detail. Note that the proposed CPDM is built upon the DDPM (Ho, Jain, and Abbeel 2020). To make the paper self-contained, we briefly introduce the mathematical background of the DDPM.

The training of DDPM consists of a forward noising process and a backward denoising process. In the forward process, noise is step-by-step added to the original sample x_0 according to a progressively increasing diffusion rate β_t ($\beta_t \in [0.0001, 0.02]$), resulting in the noisy image x_t having a distribution that is closer and closer to the standard Gaussian distribution. The forward diffusion process is defined as a Markov chain, which can be written as

$$q(x_{1:T}|x_0) := \prod_{t=1}^{T} q(x_t|x_{t-1}), \qquad (1)$$

$$q(x_t|x_{t-1}) := \mathcal{N}(x_t; \sqrt{(1-\beta_t)}x_{t-1}, \beta_t \mathbf{I}), \qquad (2)$$

where $t \in [1, T]$ denotes the current time step of the diffusion process and T represents the total number of diffusion steps. By defining $\alpha_t := 1 - \beta_t$ and $\bar{\alpha}_t := \prod_{i=1}^{t} \alpha_i$, the probability distribution $q(x_t|x_0)$ can be expressed as

$$q(x_t|x_0) = \mathcal{N}(x_t; \sqrt{\bar{\alpha}_t}x_0, (1 - \bar{\alpha}_t)\mathbf{I}). \qquad (3)$$

The sampled value x_t at time step t for a given raw image x_0 can be expressed as

$$x_t = \sqrt{\bar{\alpha}_t}x_0 + \sqrt{1 - \bar{\alpha}_t}\epsilon, \quad \epsilon \sim \mathcal{N}(0, \mathbf{I}). \qquad (4)$$

According to the computation of x_t, we can obtain that as T becomes large, the value of $\sqrt{\bar{\alpha}_t}$ approaches 0, and thus x_t tends to ϵ.

In the denoising process, solving the posterior distribution $p(x_{t-1}|x_t)$ is challenging. In practice, we can employ a neural network (denoted as θ) to approximate this distribution, and the predicted distribution is denoted as $p_\theta(x_{t-1}|x_t)$. Assuming that the mean and variance of $p_\theta(x_{t-1}|x_t)$ are $\mu_\theta(x_t, t)$ and $\sigma_\theta(x_t, t)$, respectively, we can express $p_\theta(x_{t-1}|x_t)$ as

$$p_\theta(x_{t-1}|x_t) = \mathcal{N}(x_{t-1}; \mu_\theta(x_t, t), \sigma_\theta(x_t, t)). \qquad (5)$$

For the forward diffusion process, it can be inferred that given x_0 and x_t, the distribution of $p(x_{t-1}|x_t, x_0)$ can be expressed as

$$p(x_{t-1}|x_t, x_0) = \mathcal{N}(x_{t-1}; \mu_t(x_t, x_0), \sigma_t), \qquad (6)$$

where $\mu_t(x_t, x_0) = \frac{\sqrt{\alpha_t}(1-\bar{\alpha}_{t-1})}{1-\bar{\alpha}_t}x_t + \frac{\sqrt{\bar{\alpha}_{t-1}}(1-\alpha_t)}{1-\bar{\alpha}_t}x_0$ and $\sigma_t = \frac{(1-\bar{\alpha}_{t-1})(1-\alpha_t)}{1-\bar{\alpha}_t}$. By working out x_0 from Equation (4) and then substituting into $\mu_t(x_t, x_0)$, we can achieve

$$\mu_t(x_t, t) = \frac{1}{\sqrt{\alpha_t}}(x_t - \frac{1-\alpha_t}{\sqrt{1-\bar{\alpha}_t}}\epsilon). \qquad (7)$$

Since the variance σ_t of $p(x_{t-1}|x_t, x_0)$ is a constant, predicting $p(x_{t-1}|x_t, x_0)$ is equivalent to estimating $\mu_t(x_t, t)$. Thus, we may employ the network model θ to parameterize $\mu_\theta(x_t, t)$ by

$$\mu_\theta(x_t, t) = \frac{1}{\sqrt{\alpha_t}}(x_t - \frac{1-\alpha_t}{\sqrt{1-\bar{\alpha}_t}}\epsilon_\theta(x_t, t)), \qquad (8)$$
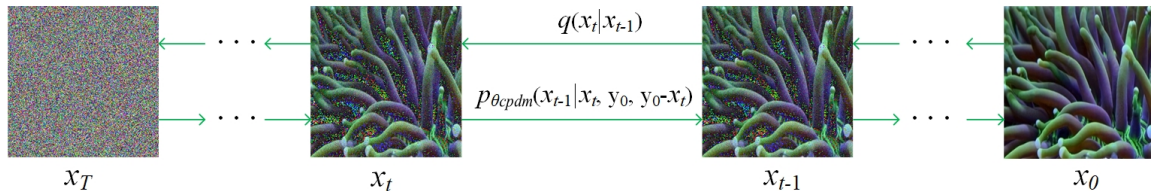
Figure 2: Illustration of our conditional input module. The forward diffusion process denotes q (from right to left), and the backward inference process denotes $p_{\theta_{cpdm}}$ (from left to right). x_0 and y_0 denote the clear and paired underwater images, respectively.

where $\epsilon_\theta(x_t, t)$ denotes the predicted value of added noise at time step t. During the training process, the goal is to make the predicted distribution $p_\theta(x_{t-1}|x_t)$ as close to the posterior $p(x_{t-1}|x_t, x_0)$ as possible. This is equivalent to minimizing $\mathbb{E}_{t,x_0,\epsilon}[||\mu_t(x_t,t) - \mu_\theta(x_t,t)||^2]$. An efficient and effective loss function for this minimization can be designed as

$$\mathcal{L}_{simple} = \mathbb{E}_{t,x_0,\epsilon}[||\epsilon - \epsilon_\theta(x_t,t)||^2]. \quad (9)$$

After the network model θ is well trained, predicting the noise introduced at time step t becomes possible. The time step t starts from 1 and gradually increases until reaching T. As T reaches a sufficiently large value, the variable x_T at time step T will follow a standard Gaussian distribution. During the sampling process, a pure noise (denoted as n_T) is sampled from the standard Gaussian distribution. Subsequently, the noise is input into the well-trained diffusion model θ. Given the input of n_t and time step t, the denoising n_{t-1} in one step can be expressed as

$$n_{t-1} = \frac{1}{\sqrt{\alpha_t}}(n_t - \frac{1-\alpha_t}{1-\sqrt{\bar{\alpha}_t}}(\epsilon_\theta(n_t,t))) + \sigma_t z, \quad (10)$$

where $z \sim \mathcal{N}(0,\mathbf{I})$. According to Equation (10), the noise caused by image degradation can be progressively removed from n_T until a meaningful image (n_0) of the target domain is generated. With the basics of the DDPM, it is convenient to illustrate how to apply the DDPM to the UIE task with two new designs. In the following, we describe each of them in detail.

Conditional Input Module

Our CPDM for underwater image enhancement differs from the fundamental diffusion model in the training and sampling processes. First, we need a paired dataset $\{(x_0^i, y_0^i)\}, i = 0, 1, ..., S$ for training, where S is the size of the dataset, y_0^i and x_0^i denote the i-th raw degraded underwater image and its corresponding clear in-air image, respectively. For simplicity, we hereinafter use the sample (x_0, y_0) to represent an arbitrary training sample (x_0^i, y_0^i). In the training process, except for the input of the noisy image (x_t), we input the raw underwater image (y_0) at each time step t as a supervisory condition, which can guide the diffusion model to generate the enhanced underwater images. Furthermore, we find that when applying to the UIE task, the diffusion model built upon the UNet (Ronneberger, Fischer, and Brox 2015) network structure is too simple to extract sufficient information from the raw image. To address this problem, an additional condition is introduced, which is the difference between the raw

underwater image (y_0) and the noisy image (x_t) at the current time step t. By incorporating this difference ($y_0 - x_t$) as another conditional input, the network can extract more useful information and cues about y_0 and x_t. The extracted information helps the diffusion model to produce more accurate and visually appealing enhancements.

After introducing our conditional input (y_0 and $y_0 - x_t$), the posterior probability of our diffusion model (denoted as θ_{cpdm}) can be defined as

$$p_{\theta_{cpdm}}(x_{t-1}|x_t, y_0, y_0 - x_t) =$$
$$\mathcal{N}(x_{t-1}; \mu_{\theta_{cpdm}}(x_t, t, y_0, y_0 - x_t), \quad (11)$$
$$\sigma_{\theta_{cpdm}}(x_t, t, y_0, y_0 - x_t)).$$

Accordingly, the mean of the predicted noise can be written as

$$\mu_{\theta_{cpdm}}(x_t, t, y_0, y_0 - x_t) =$$
$$\frac{1}{\sqrt{\alpha_t}}(x_t - \frac{1-\alpha_t}{\sqrt{1-\bar{\alpha}_t}}\epsilon_{\theta_{cpdm}}(x_t, t, y_0, y_0 - x_t)). \quad (12)$$

Therefore, our loss function $\mathcal{L}_{cpdm}$ can be defined as

$$\mathcal{L}_{cpdm} = \mathbb{E}_{t,x_0,y_0,\epsilon}[||\epsilon - \epsilon_{\theta_{cpdm}}(x_t, t, y_0, y_0 - x_t)||^2]. \quad (13)$$

Content Compensation Module

In this part, we introduce a content compensation module to boost the ability of the information aggregation inside the noise prediction network. It is known that the UNet depends on a relatively straightforward network structure, and the UIE task demands the safeguarding of vital low-level features, including color, contour, edge, texture, and shape. On this basis, our content compensation module seamlessly integrates the low-level information extracted from the raw image y_0 into each layer of the UNet network. The training framework for time step t is illustrated in Figure 3. As shown in Figure 3, each layer of our UNet has four blocks, and the content compensation module inputs a low-level feature of the raw image into the last block of each layer in the encoder side (i.e., downsampling part). Such low-level features can always control the network to preserve the image content, which is beneficial to restore a high-quality target image corresponding to the input raw underwater image. The significance of the content compensation module lies in its ability to effectively retain the low-level features during the sampling process, thereby leading to an overall enhancement in the quality of the restored image. Algorithm 1 and Algorithm 2 illustrate our training and sampling processes, respectively.
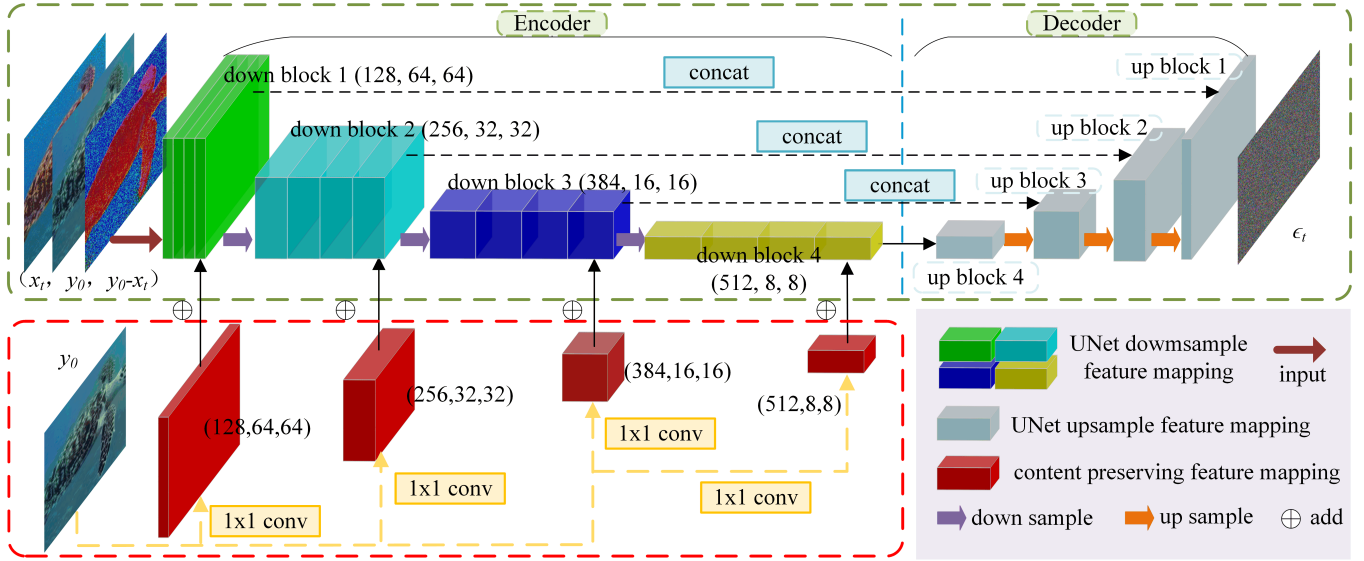
Figure 3: Illustration of the proposed CPDM at time step t. Here, y_0 represents the to-be-enhanced underwater image, and x_t denotes the noisy image of the current time step.

Methods	Test_L400			Test_U90			Test_E200		
	PSNR ↑	SSIM ↑	MSE ↓	PSNR ↑	SSIM ↑	MSE ↓	PSNR ↑	SSIM ↑	MSE ↓
WaterNet (Li et al. 2019)	19.53	0.84	0.0188	16.89	0.73	0.0299	17.44	0.74	0.0253
FUnIE (Islam, Xia, and Sattar 2020)	23.46	0.86	0.0115	18.46	0.74	0.0276	22.24	0.88	0.0086
Ucolor (Li et al. 2021)	21.77	0.88	0.0092	20.59	0.83	0.0132	21.45	0.86	0.0092
Restormer (Zamir et al. 2022)	20.57	0.84	0.0178	18.57	0.73	0.0232	19.08	0.83	0.0215
Maxim (Tu et al. 2022)	19.93	0.78	0.0121	17.14	0.76	0.0267	18.05	0.72	0.0234
U-shape (Peng, Zhu, and Bian 2023)	24.24	**0.89**	0.0065	20.07	0.78	0.0137	22.05	0.86	0.0089
CPDM (Ours)	**25.11**	0.88	**0.0056**	**21.07**	**0.84**	**0.0114**	**23.24**	**0.90**	**0.0062**

Table 1: Quantitative comparison of different UIE methods on the LSUI, UIEB, and EUVP datasets. The best results are highlighted in bold.

Algorithm 1: Training a denoising model $\epsilon_{\theta_{cpdm}}$

1: **Repeat**
2: $(x_0, y_0) \sim q(x_0^i, y_0^i)$
3: $t \sim \text{Uniform}(\{1, \ldots, T\})$
4: $\epsilon \sim \mathcal{N}(0, \mathbf{I})$
5: Take gradient descent step on
    $\nabla_\theta \|\epsilon - \epsilon_{\theta_{cpdm}}(x_0, t, y_0, y_0 - x_t)\|^2$
6: **Until** converged

Algorithm 2: Sampling for condition y_0

1: **Sample** $x_T \sim \mathcal{N}(0, \mathbf{I})$ and y_0
2: **for** $t = T, \ldots, 1$ **do**
3: $z \sim \mathcal{N}(\mathbf{0}, \mathbf{I})$ if $t > 1$, else $z = \mathbf{0}$
4: $x_{t-1} = \frac{1}{\sqrt{\alpha_t}}(x_t - \frac{1-\alpha_t}{1-\sqrt{\bar{\alpha}_t}}(\epsilon_{\theta_{cpdm}}(x_t, t, y_0, y_0 - x_t))) + \sigma_t z$
5: **end for**
6: **Return** x_0

Experiments

Dataset

Large Scale Underwater Image Dataset (LSUI) (Peng, Zhu, and Bian 2023) contains 4,279 image pairs. This dataset involves a rich range of underwater scenes (lighting conditions, water body types, and target categories) with good visual quality. We divide the LSUI into 3,879 pairs of training data (Train_L) and 400 pairs of test data (Test_L400). In addition, an Underwater Image Enhancement Benchmark (UIEB) dataset (Li et al. 2019) is also used in our experiment. This

dataset contains 890 data pairs, where 800 pairs are used for training, and the remaining 90 pairs are used for testing (Test_U90). In addition to these two datasets, we select 200 pairs of underwater images from the Enhancing Underwater Visual Perception dataset (EUVP) (Islam, Xia, and Sattar 2020) for out-of-sample testing. This additional test dataset is referred to as Test_E200. To facilitate the training of our diffusion model, we resize all image pairs into 64×64 size.

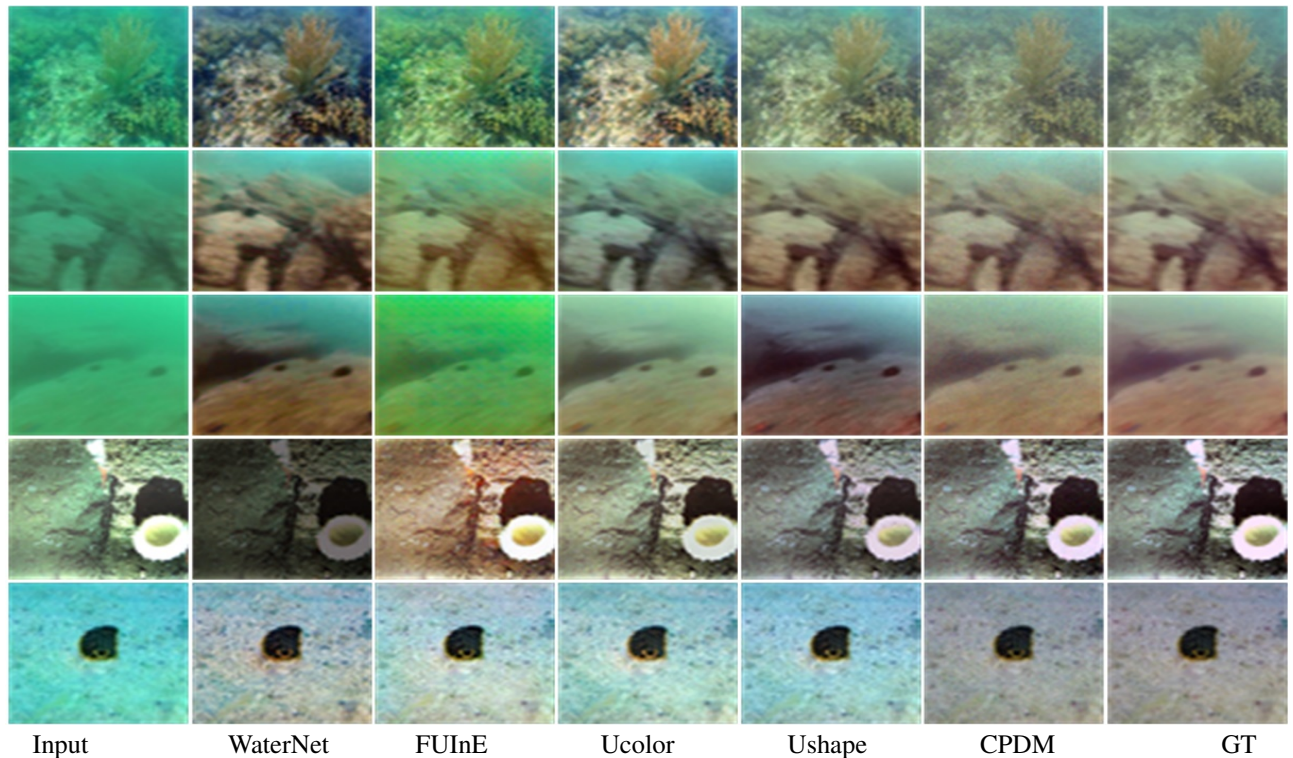| Input | WaterNet | FUInE | Ucolor | Ushape | CPDM | GT |

Figure 4: Visual comparison of enhanced underwater images by various methods on the Test_L400 (LSUI) dataset. From left to right: original underwater image, results from WaterNet (Li et al. 2019), FUnIE (Islam, Xia, and Sattar 2020), Ucolor (Li et al. 2021), U-shape Transformer (Peng, Zhu, and Bian 2023), our CPDM method, and the reference image.

Experimental Setting and Metrics

Our experiments are run on an RXT 3090 GPU. In the forward process, we set $T = 1000$. Since the test dataset contains the reference images, we can compute the full-reference quality evaluation metrics such as PSNR (Korhonen and You 2012), SSIM (Horé and Ziou 2010), and MSE (Li et al. 2019). These three metrics reflect the proximity to the reference, with higher PSNR values representing closer image content, higher SSIM values reflecting more similar structures and textures, and lower MSE values indicating smaller differences between the corresponding pixels of two images. Six mainstream UIE methods including WaterNet (Li et al. 2019), FUnIE (Islam, Xia, and Sattar 2020), Ucolor (Li et al. 2021), Restormer (Zamir et al. 2022), Maxim (Tu et al. 2022), and U-shape Transformer (Peng, Zhu, and Bian 2023) are selected for the performance comparison.

Results

As shown in Table 1, our Content-Preserving Diffusion Model (CPDM) method achieves promising results in quantitative metrics (PSNR, SSIM, and MSE). Specifically, on Test_U90, our method outperforms all the compared methods in the three metrics. On Test_L400, our method obtains 3.6% improvement in PSNR, while exhibiting a bit slight decrease in SSIM compared to its best competitor. Furthermore, on Test_E200, our CPDM method consistently outperforms all the competing techniques. Note that we conduct an extra test

on the Test_E200 dataset, without prior training on the EUVP dataset. This test can verify the generalization ability of the compared methods. As shown in Figures 4 and 5, our CPDM method produces better visual results that are much closer to the reference images than its competitors. In particular, we can see from Figure 4 that the enhanced images by our method preserve better color consistency with the reference ones compared to other methods. Regarding the luminance restoration, it can be observed from Figure 5 that our CPDM achieves an obvious advantage over the compared methods.

The superior performance of our CPDM can be attributed to two key designs: conditional input module and content compensation module. Firstly, we introduce the conditional input during the training of the noise prediction network. By introducing the raw image and the difference between the raw image and the noisy image of the current time step as conditional input, the noise prediction model can iteratively refine useful characteristics from the conditional input. Through this step-by-step refinement, our method can restore high-quality target images. Secondly, the content compensation module plays a pivotal role in extracting the low-level features of the input images, as depicted in Figure 3. By integrating such features into the UNet network, the content compensation module ensures that the enhanced images possess the same content information as the raw images, such as edge, texture, and shape, throughout the sampling process. This preservation of low-level features contributes significantly to the overall improvement in the quality of the enhanced
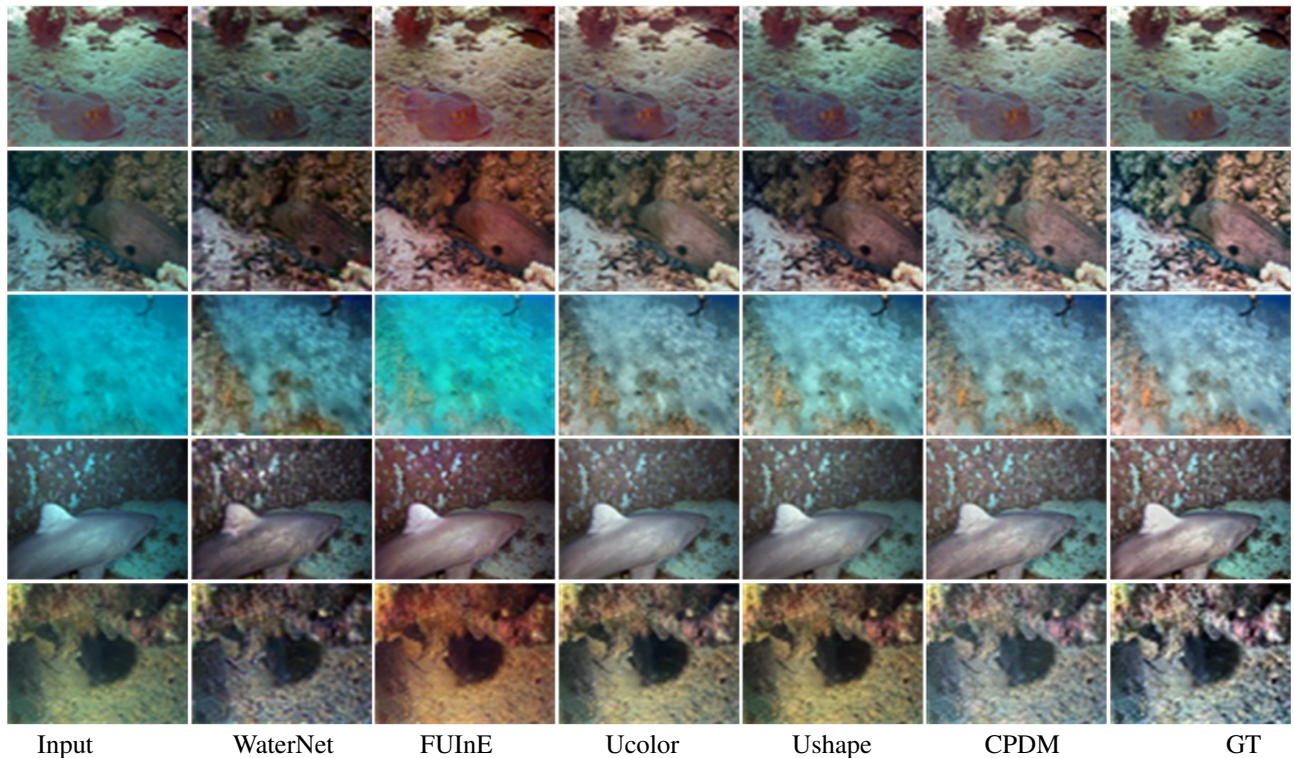
| | Input | WaterNet | FUInE | Ucolor | Ushape | CPDM | GT |

Figure 5: Visual comparison of enhanced underwater images by various methods on the Test_U90 (UIEB) dataset. From left to right: original underwater image, results from WaterNet (Li et al. 2019), FUnIE (Islam, Xia, and Sattar 2020), Ucolor (Li et al. 2021), U-shape Transformer (Peng, Zhu, and Bian 2023), our CPDM method, and the reference image.

images.

Models	Test_L400			Test_U90		
	PSNR ↑	SSIM ↑	MSE ↓	PSNR ↑	SSIM ↑	MSE ↓
model-A	24.01	0.87	0.0074	19.95	0.80	0.0164
model-B	24.72	**0.88**	0.0063	20.31	0.80	0.0153
model-C	24.26	0.87	0.0073	21.03	0.82	0.0129
model-D	**25.11**	**0.88**	**0.0056**	**21.07**	**0.84**	**0.0114**

Table 2: Ablation study on the Test_L400 and Test_U90 datasets. Here, model-A represents only inputting y_0 as the input condition, model-B represents inputting both y_0 and y_0-x_t as the input conditions, model-C represents inputting both y_0 and content compensation module as the input conditions, and model-D represents a full model.
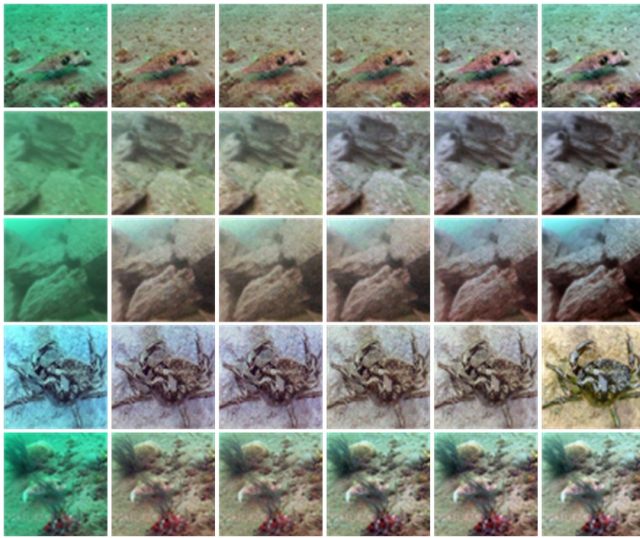
Ablation Study

To verify the effectiveness of each module designed in our method, we conduct a series of ablation experiments in a step-by-step addition manner. This way allows us to gradually assess the contribution of each module to the overall performance of CPDM. The numerical results of these ablation experiments are summarized in Table 2, and the corresponding visualization effects are shown in Figure 6.

Base Model. The visual effects show that utilizing only the raw image as the input condition (model-A) can produce

semantically meaningful results. This showcases a certain potential of diffusion-based methods for enhancing underwater images. However, we can see from Table 2 that its numerical results arrive at the lowest level in all objective metrics.

Model with Conditional Input Module. The performance of model-B is improved when the offset between the raw image and the noisy image of the current time step is added as the conditional input. Adding the dual-input condition significantly enhances the model's overall performance. Compared to model-A, incorporating the offset between the raw image and the noisy image of the current time step in model-B allows for further integration of the information of x_t predicted at the current time step. As shown in Figure 6, the output images of model-B exhibit improved consistency in terms of color tone compared to those of model-A. Furthermore, as indicated by the quantitative metrics in Table 2, model-B outperforms model-A in objective metrics. Our designed conditional input module incorporates the $y_0 - x_t$ of the current time step as a conditional input into the diffusion model. Compared to the raw diffusion model, including a conditional input related to x_t provides additional complementary information to the model. Thus, our designed conditional input module is proven to be beneficial for conditional diffusion tasks.

Model with Content Compensation Module. To validate the functionality of our designed content compensation module, we introduce model-C, which incorporates both

| Input | model-A | model-B | model-C | model-D | GT |

Figure 6: Comparison of visual effects on the Test_L400 dataset in the ablation study.

y_0 and the content compensation module as inputs. Unlike model-B, model-C removes the input $y_0 - x_t$ and includes a content compensation module instead. As shown in Figure 6, we can observe that all our models achieve good visual results, including model-A, model-B, and model-C. Interestingly, model-C exhibits improved color consistency closer to the real reference images than model-A and model-B. As presented in Table 2, model-C outperforms models-A and model-B in terms of numerical results. The design of model-C incorporates the content compensation module on top of model-A. Our designed content compensation module can extract structural information from the input y_0 across different feature dimensions, which is then fed into different layers of the UNet architecture. This further enhances the encoding of input information and decoding of output in the UNet framework. Therefore, our designed content compensation module is also proven to be beneficial for conditional diffusion tasks.

Full Model. Finally, we can see that the full model (model-D) encompassing all modules achieves the best results. This outcome indicates that each module of the CPDM plays a specific role and contributes to its overall effectiveness. The step-by-step addition of these modules gradually enhances the model's capability, leading to improved image quality in the UIE task.

Conclusion

In the article, we have attempted to adapt the diffusion model to the underwater image enhancement (UIE) task and have presented a Content-Preserving Diffusion Model (CPDM) for enhancing the quality of the restored underwater image. The proposed CPDM has demonstrated impressive performance compared with the leading UIE methods. We introduce two carefully designed conditional inputs, effectively guiding CPDM to generate high-quality results. Moreover, our designed content compensation module plays a crucial role throughout the training process, ensuring the content preservation of the raw image. Our CPDM works in an iterative refinement paradigm by embedding two modules into each time step in both the training and sampling processes, thereby preserving the image content in each denoising step and enhancing the quality of the restored images. Extensive experimental results validate the outstanding capabilities of CPDM in terms of numerical evaluations and visual effects. More importantly, the methodology designed in our CPDM can be easily extended to other conditional generative tasks.

References

Ahn, J.; Yasukawa, S.; Sonoda, T.; Ura, T.; and Ishii, K. 2017. Enhancement of deep-sea floor images obtained by an underwater vehicle and its evaluation by crab recognition. *Journal of Marine Science and Technology*, 22: 758–770.

Akkaynak, D.; and Treibitz, T. 2018. A revised underwater image formation model. In *IEEE Conference on Computer Vision and Pattern Recognition*, 6723–6732.

Akkaynak, D.; and Treibitz, T. 2019. Sea-thru: A method for removing water from underwater images. In *IEEE Conference on Computer Vision and Pattern Recognition*, 1682–1691.

Akkaynak, D.; Treibitz, T.; Shlesinger, T.; Loya, Y.; Tamir, R.; and Iluz, D. 2017. What is the space of attenuation coefficients in underwater computer vision? In *IEEE Conference on Computer Vision and Pattern Recognition*, 4931–4940.

Croitoru, F.-A.; Hondru, V.; Ionescu, R. T.; and Shah, M. 2023. Diffusion models in vision: A survey. *IEEE Transactions on Pattern Analysis and Machine Intelligence*, 45(9): 10850–10869.

Dhariwal, P.; and Nichol, A. 2021. Diffusion models beat gans on image synthesis. *Advances in Neural Information Processing Systems*, 34: 8780–8794.

Drews, P. L.; Nascimento, E. R.; Botelho, S. S.; and Campos, M. F. M. 2016. Underwater depth estimation and image restoration based on single images. *IEEE Computer Graphics and Applications*, 36(2): 24–35.

Fu, Z.; Lin, X.; Wang, W.; Huang, Y.; and Ding, X. 2022. Underwater image enhancement via learning water type desensitized representations. In *IEEE International Conference on Acoustics, Speech and Signal Processing*, 2764–2768.

Galdran, A.; Pardo, D.; Picón, A.; and Alvarez-Gila, A. 2015. Automatic red-channel underwater image restoration. *Journal of Visual Communication and Image Representation*, 26: 132–145.

Goodfellow, I.; Pouget-Abadie, J.; Mirza, M.; Xu, B.; Warde-Farley, D.; Ozair, S.; Courville, A.; and Bengio, Y. 2014. Generative adversarial nets. *Advances in Neural Information Processing Systems*, 2672–2680.

Guo, Y.; Li, H.; and Zhuang, P. 2019. Underwater image enhancement using a multiscale dense generative adversarial network. *IEEE Journal of Oceanic Engineering*, 45(3): 862–870.

Ho, J.; Jain, A.; and Abbeel, P. 2020. Denoising diffusion probabilistic models. *Advances in Neural Information Processing Systems*, 33: 6840–6851.

Horé, A.; and Ziou, D. 2010. Image quality metrics: PSNR vs. SSIM. In *20th International Conference on Pattern Recognition*, 2366–2369.

Hou, W.; Woods, S.; Jarosz, E.; Goode, W.; and Weidemann, A. 2012. Optical turbulence on underwater image degradation in natural environments. *Applied Optics*, 51(14): 2678–2686.

Islam, M. J.; Xia, Y.; and Sattar, J. 2020. Fast underwater image enhancement for improved visual perception. *IEEE Robotics and Automation Letters*, 5(2): 3227–3234.

Jaffe, J. S. 1990. Computer modeling and the design of optimal underwater imaging systems. *IEEE Journal of Oceanic Engineering*, 15(2): 101–111.

Jarzynski; and C. 1997. Equilibrium free energy differences from nonequilibrium measurements: a master equation approach. *Physical Review E*, 56(5): 5018–5035.

Johnsen, G.; Ludvigsen, M.; Sørensen, A.; and Aas, L. M. S. 2016. The use of underwater hyperspectral imaging deployed on remotely operated vehicles-methods and applications. *IFAC-PapersOnLine*, 49(23): 476–481.

Korhonen, J.; and You, J. 2012. Peak signal-to-noise ratio revisited: Is simple beautiful? In *Fourth International Workshop on Quality of Multimedia Experience*, 37–38.

Li, C.; Anwar, S.; Hou, J.; Cong, R.; Guo, C.; and Ren, W. 2021. Underwater image enhancement via medium transmission-guided multi-color space embedding. *IEEE Transactions on Image Processing*, 30: 4985–5000.

Li, C.; Guo, C.; Ren, W.; Cong, R.; Hou, J.; Kwong, S.; and Tao, D. 2019. An underwater image enhancement benchmark dataset and beyond. *IEEE Transactions on Image Processing*, 29: 4376–4389.

Li, C.; Guo, J.; and Guo, C. 2018. Emerging from water: Underwater image color correction based on weakly supervised color transfer. *IEEE Signal Processing Letters*, 25(3): 323–327.

Li, C.; Guo, J.; Guo, C.; Cong, R.; and Gong, J. 2017a. A hybrid method for underwater image correction. *Pattern Recognition Letters*, 94: 62–67.

Li, C.-Y.; Guo, J.-C.; Cong, R.-M.; Pang, Y.-W.; and Wang, B. 2016. Underwater image enhancement by dehazing with minimum information loss and histogram distribution prior. *IEEE Transactions on Image Processing*, 25(12): 5664–5677.

Li, J.; Skinner, K. A.; Eustice, R. M.; and Johnson-Roberson, M. 2017b. WaterGAN: Unsupervised generative network to enable real-time color correction of monocular underwater images. *IEEE Robotics and Automation Letters*, 3(1): 387–394.

Li, S.; Higashita, R.; Fu, H.; Li, H.; Niu, J.; and Liu, J. 2023. Content-Preserving Diffusion Model for Unsupervised AS-OCT image Despeckling. arXiv:2306.17717.

Liu, H.; and Chau, L.-P. 2016. Underwater image restoration based on contrast enhancement. In *IEEE International Conference on Digital Signal Processing*, 584–588.

Liu, X.; Park, D. H.; Azadi, S.; Zhang, G.; Chopikyan, A.; Hu, Y.; Shi, H.; Rohrbach, A.; and Darrell, T. 2023. More control for free! image synthesis with semantic diffusion guidance. In *IEEE Winter Conference on Applications of Computer Vision*, 289–299.

Ludvigsen, M.; Sortland, B.; Johnsen, G.; and Singh, H. 2007. Applications of geo-referenced underwater photo mosaics in marine biology and archaeology. *Oceanography*, 20(4): 140–149.

McGlamery, B. 1980. A computer model for underwater camera systems. In *Ocean Optics VI*, volume 208, 221–231.

Paulo Drews, J. R.; Nascimento, E.; Moraes, F.; Botelho, S.; and Campos, M. 2013. Transmission Estimation in Underwater Single Images. In *IEEE International Conference on Computer Vision Workshops*, 825–830.

Peng, L.; Zhu, C.; and Bian, L. 2023. U-shape transformer for underwater image enhancement. *IEEE Transactions on Image Processing*, 32: 3066–3079.

Peng, Y.-T.; Cao, K.; and Cosman, P. C. 2018. Generalization of the dark channel prior for single image restoration. *IEEE Transactions on Image Processing*, 27(6): 2856–2868.

Peng, Y.-T.; and Cosman, P. C. 2017. Underwater image restoration based on image blurriness and light absorption. *IEEE Transactions on Image Processing*, 26(4): 1579–1594.

Ronneberger, O.; Fischer, P.; and Brox, T. 2015. U-net: Convolutional networks for biomedical image segmentation. In *Medical Image Computing and Computer-Assisted Intervention*, 234–241.

Sohl-Dickstein, J.; Weiss, E. A.; Maheswaranathan, N.; and Ganguli, S. 2015. Deep Unsupervised Learning using Nonequilibrium Thermodynamics. In *International Conference on Machine Learning*, 2256–2265.

Song, J.; Meng, C.; and Ermon, S. 2020. Denoising diffusion implicit models. In *International Conference on Learning Representations*.

Strachan, N. 1993. Recognition of fish species by colour and shape. *Image and Vision Computing*, 11(1): 2–10.

Tu, Z.; Talebi, H.; Zhang, H.; Yang, F.; Milanfar, P.; Bovik, A.; and Li, Y. 2022. Maxim: Multi-axis mlp for image processing. In *IEEE Conference on Computer Vision and Pattern Recognition*, 5769–5780.

Wang, Y.; Liu, H.; and Chau, L.-P. 2017. Single underwater image restoration using adaptive attenuation-curve prior. *IEEE Transactions on Circuits and Systems I: Regular Papers*, 65(3): 992–1002.

Yang, M.; Hu, K.; Du, Y.; Wei, Z.; and Hu, J. 2019. Underwater image enhancement based on conditional generative adversarial network. *Signal Processing Image Communication*, 81.

Zamir, S. W.; Arora, A.; Khan, S.; Hayat, M.; Khan, F. S.; and Yang, M.-H. 2022. Restormer: Efficient transformer for high-resolution image restoration. In *IEEE Conference on Computer Vision and Pattern Recognition*, 5728–5739.